Polarization Selection Rules for Inter-Landau-Level Transitions in Epitaxial Graphene Revealed by the Infrared Optical Hall Effect

P Kuehne, Vanya Darakchieva, Rositsa Yakimova, J D. Tedesco, R L. Myers-Ward, C R. Jr Eddy, D K. Gaskill, C M. Herzinger, J A. Woollam, M Schubert and T Hofmann

Original Publication:

P Kuehne, Vanya Darakchieva, Rositsa Yakimova, J D. Tedesco, R L. Myers-Ward, C R. Jr Eddy, D K. Gaskill, C M. Herzinger, J A. Woollam, M Schubert and T Hofmann, Polarization Selection Rules for Inter-Landau-Level Transitions in Epitaxial Graphene Revealed by the Infrared Optical Hall Effect, 2013, Physical Review Letters, (111), 7, e077402.
http://dx.doi.org/10.1103/PhysRevLett.111.077402

Polarization Selection Rules for Inter-Landau-Level Transitions in Epitaxial Graphene Revealed by the Infrared Optical Hall Effect

P. Kühne,[1,*] V. Darakchieva,[2] R. Yakimova,[2] J. D. Tedesco,[3] R. L. Myers-Ward,[4] C. R. Eddy, Jr.,[4] D. K. Gaskill,[4] C. M. Herzinger,[5] J. A. Woollam,[5] M. Schubert,[1] and T. Hofmann[1]

[1]*Department of Electrical Engineering and Center for Nanohybrid Functional Materials, University of Nebraska-Lincoln, Lincoln, Nebraska 68588, USA*

[2]*Department of Physics, Chemistry and Biology, IFM, Linköping University, SE-581 83 Linköping, Sweden*

[3]*ABB, Inc., 171 Industry Drive, Post Office Box 38, Bland, Virginia 24315, USA*

[4]*U.S. Naval Research Laboratory, Washington, D.C. 20375, USA*

[5]*J. A. Woollam Co., Inc., 645 M Street, Suite 102, Lincoln, Nebraska 68508-2243, USA*

(Received 1 April 2013; revised manuscript received 7 May 2013; published 14 August 2013)

We report on the polarization selection rules of inter-Landau-level transitions using reflection-type optical Hall effect measurements from 600 to 4000 cm^{-1} on epitaxial graphene grown by thermal decomposition of silicon carbide. We observe symmetric and antisymmetric signatures in our data due to polarization preserving and polarization mixing inter-Landau-level transitions, respectively. From field-dependent measurements, we identify that transitions in coupled graphene monolayers are governed by polarization mixing selection rules, whereas transitions in decoupled graphene monolayers are governed by polarization preserving selection rules. The selection rules may find explanation by different coupling mechanisms of inter-Landau-level transitions with free charge carrier magneto-optic plasma oscillations.

DOI: 10.1103/PhysRevLett.111.077402 PACS numbers: 78.67.Wj, 71.70.Di, 76.40.+b, 77.22.Ej

Epitaxial graphene grown by thermal decomposition onto SiC substrates has received tremendous interest due to its unique physical and electronic properties where free charge carriers behave as quasi-Dirac particles, for instance [1–12]. Infrared magneto-optic spectroscopy has been widely applied to probe the electronic states of graphene by monitoring the magnetic field and frequency dependencies of inter-Landau-level transitions (LL) [1,2,13–15]. However, the polarization properties of inter-Landau-level transitions and their polarization selection rules, that is, whether individual transitions are polarization preserving or polarization mixing, are unknown. The polarization selection rules determine the symmetry properties of the magneto-optic dielectric permittivity tensor $\boldsymbol{\varepsilon}^{\mathrm{MO}}$. For a given series of inter-Landau-level transitions, $\boldsymbol{\varepsilon}^{\mathrm{MO}}$ can be constructed and compared with physical model descriptions. Sufficient information for obtaining the polarization selection rules and to construct $\boldsymbol{\varepsilon}^{\mathrm{MO}}$ is provided by optical Hall effect measurements [16,17] and is presented in this Letter. We report here on our observation of isotropic and anisotropic inter-Landau-level transitions from optical Hall effect measurements which differ in their magnetic field dependencies, and we discuss possible physical origins by reconstructing $\boldsymbol{\varepsilon}^{\mathrm{MO}}$ using simple model scenarios.

The optical Hall effect determines changes of optical properties of thin film samples under the influence of external magnetic fields [17–19]. In contrast to Faraday rotation, measurements are conveniently taken in reflection-type arrangement at oblique angle of incidence, thereby discriminating between parallel and perpendicular polarization. Measurements are performed in the Stokes vector approach, and results are reported in the Mueller matrix presentation, which allows immediate differentiation between polarization preserving (isotropic) as well as polarization mixing (anisotropic) sample properties. Subsequent data analysis using model approaches for the dielectric function, or equivalently the optical conductivity, permits quantitative access to physical model parameters. In the Stokes formalism, the Mueller matrix $\mathbf{M}$ connects the Stokes vector of incident and reflected electromagnetic waves $\mathbf{S}^{\mathrm{in}}$ and $\mathbf{S}^{\mathrm{out}}$, respectively, where $\mathbf{S}^{\mathrm{out}} = \mathbf{M}\mathbf{S}^{\mathrm{in}}$ [20]. The optical Hall effect determines magnetic field-induced differences $\delta\mathbf{M}$ with respect to $\mathbf{M}$ at zero field. $\delta\mathbf{M}$ contains nonzero on-diagonal-block elements only (δM_{11}, δM_{12}, δM_{21}, δM_{22}, δM_{33}, δM_{34}, δM_{43}, and δM_{44}) when the magnetic field-induced sample response is purely isotropic; i.e., no polarization mixing occurs. Additional, nonzero off-diagonal-block elements occur (δM_{13}, δM_{31}, δM_{14}, δM_{41}, δM_{23}, δM_{32}, δM_{24}, and δM_{42}) when the magnetic field-induced sample response is anisotropic; i.e., polarization mode mixing occurs [20]. Therefore, symmetric signatures of inter-Landau-level transitions occur within the on-diagonal-block elements only. Antisymmetric signatures also occur within all off-diagonal-block elements. We note that in our setup, elements of both the fourth row and column are inaccessible, and all remaining elements are normalized by M_{11} removing light source base line fluctuations, providing eight independent pieces of information.

The epitaxial graphene sample investigated in this Letter was grown by sublimation on the C-polar $(000\bar{1})$ surface

of a semi-insulating 6H-SiC substrate. During the growth, the SiC substrate was heated to 1400 °C in an argon atmosphere. Further information on growth conditions can be found in Ref. [21]. We estimate the number of graphene layers to be 10–20, similar to those measured previously on C-face 4H-SiC [22]. Optical Hall effect measurements were carried out at a $\Phi_a = 45°$ angle of incidence in the spectral range from 600 to 4000 cm^{-1} with a spectral resolution of 1 cm^{-1} [16]. The sample was held at temperature $T = 1.5$ K. The magnetic field was varied from $B = 0$ to 8 T in 0.1 T increments while the magnetic field direction was parallel to the reflected beam, resulting in a magnetic field $B_c = B/\sqrt{2}$ parallel to the sample normal.

Quantitative optical Hall effect data analysis requires stratified layer model calculations in which parametrized dielectric functions are used. Least-square principle methods are employed in order to vary model parameters until calculated and experimental ellipsometric data are matched as closely as possible (best model) [23]. The dielectric functions for silicon carbide are composed of Lorentzian-broadened oscillators described by the respective longitudinal-optical and transverse-optical phonon frequencies [24].

Figure 1 depicts results of optical Hall effect measurements at $B_c = +(5.66 \pm 0.02)$ T. Graphs are arranged according to their appearance in the Mueller matrix, with the top left corner (δM_{11}) omitted. The spectral response observed in the on-diagonal-block elements is distinctly different from the off-diagonal-block response. Multiple transitions with different polarization signatures can be identified. Sets of signatures belong to different series of inter-Landau-level transitions, as will be discussed below. Comparing representative elements, e.g., δM_{33} and δM_{32}, two sets with different polarization properties can be identified. The first set of transitions, indicated with vertical arrows labeled LL_{SLG}, is isotropic, i.e., not associated with polarization mixing, and spread out over the entire measured spectral range. These transitions do not occur in off-diagonal-block elements. The term SLG stands for single-layer graphene, as discussed further below. The second set of resonances, indicated with vertical arrows labeled LL_{BLG}, is anisotropic, i.e., associated with polarization mixing, and occurs in a narrower range from 600 to 1500 cm^{-1}. The term BLG indicates bilayer graphene, as discussed further below as well. However, a subset of these transitions will be assigned to trilayer graphene. In addition, a pronounced feature observed at 970 cm^{-1}, indicated with vertical arrows and labeled by DTC, is common to all graphs in Fig. 1 and hence anisotropic. The term DTC stands for Drude-type carriers. Nonzero off-diagonal-block

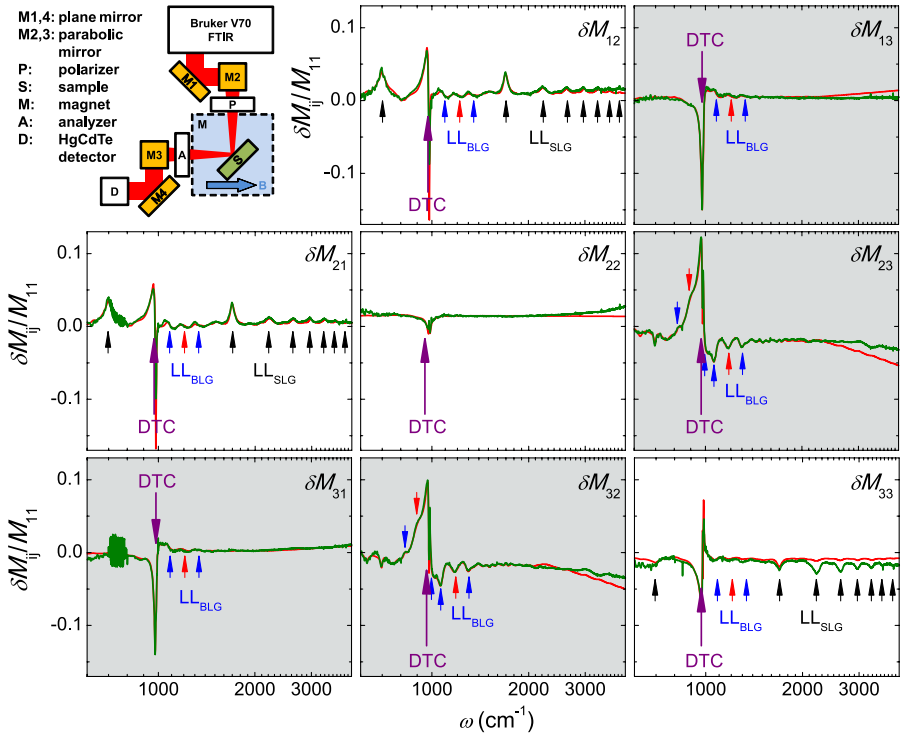

FIG. 1 (color online). Optical Hall effect experimental data (green, dotted lines) and best-model fit data (red, solid lines) for epitaxial graphene at $B_c = +(5.66 \pm 0.02)$ T and $T = 1.5$ K. The angle of incidence is $\Phi_a = 45°$. DTC, BLG, and SLG denote contributions assigned in this Letter to Drude-type carriers, bilayer graphene LL, and single-layer graphene LL, respectively. Signatures indicated by SLG are isotropic and do not occur in off-diagonal-block elements δM_{13}, δM_{23}, δM_{31}, and δM_{32} (shaded background), while features labeled with DTC and BLG are anisotropic and cause polarization mixing. A schematic representation of the optical Hall effect experimental setup is given in the left upper corner.

Mueller matrix elements are inherently tied to the existence of off-diagonal components in $\boldsymbol{\varepsilon}^{\mathrm{MO}}$. Thus, *a priori*, one must conclude that transitions $\mathrm{LL}_{\mathrm{SLG}}$ originate from processes in sample regions with polarizability contributions to $\boldsymbol{\varepsilon}^{\mathrm{MO}}$ that are diagonal in $\boldsymbol{\varepsilon}^{\mathrm{MO}}$ and hence isotropic. Likewise, transitions $\mathrm{LL}_{\mathrm{BLG}}$ are to be described by contributions with nondiagonal components in $\boldsymbol{\varepsilon}^{\mathrm{MO}}$.

Without loss of generality, the optical response of electronic systems with bound and unbound excitations subjected to external magnetic fields can be constructed by using magneto-optic polarizability functions χ_+ and χ_- for right- and left-handed circularly polarized light, respectively [18]. In Cartesian coordinates, $\boldsymbol{\varepsilon}^{\mathrm{MO}}$ is then antisymmetric:

$$\boldsymbol{\varepsilon}^{\mathrm{MO}} = \mathbf{I} + \frac{1}{2}\begin{pmatrix} (\chi_+ + \chi_-) & i(\chi_+ - \chi_-) & 0 \\ -i(\chi_+ - \chi_-) & (\chi_+ + \chi_-) & 0 \\ 0 & 0 & 0 \end{pmatrix}, \quad (1)$$

where $\mathbf{I}$ indicates the unit matrix and the magnetic field is taken along the z direction. All other dielectric contributions are omitted. For $\chi_+ \neq \chi_-$, $\boldsymbol{\varepsilon}^{\mathrm{MO}}$ describes a medium with anisotropic magneto-optical properties which produce nonvanishing off-diagonal-block elements in the optical Hall effect, whereas for $\chi_+ = \chi_-$, $\boldsymbol{\varepsilon}^{\mathrm{MO}}$ describes a medium with isotropic magneto-optical properties, and off-diagonal-block elements in the optical Hall effect do not occur. Hence, for transitions $\mathrm{LL}_{\mathrm{SLG}}$, $\chi_+ = \chi_-$, while for $\mathrm{LL}_{\mathrm{BLG}}$, $\chi_+ \neq \chi_-$. A semiclassical description for $\chi_\pm$ can be obtained using n series of Lorentzian-broadened Green functions at energies $\hbar\omega_{0,n}$ with spectral weight $\omega_{p,n}^2$, scattering life time $1/\gamma_n$, and including coupling to a magneto-optic plasma mode ω_c

$$\chi_\pm = \sum_n \omega_{p,n}^2(\omega_{0,n}^2 - \omega^2 - i\omega\gamma_{p,n} \pm i\omega\omega_c)^{-1}. \quad (2)$$

When the plasma coupling is turned off, i.e., $\omega_c \to 0$, $\boldsymbol{\varepsilon}^{\mathrm{MO}}$ becomes symmetric. Standard layer model calculations to determine the Mueller matrix elements of epitaxial graphene on silicon carbide using Eqs. (1) and (2) reproduce the line shape and isotropy of all features labeled $\mathrm{LL}_{\mathrm{SLG}}$ in Fig. 1. When coupling with plasma modes is considered, i.e., $\omega_c > 0$, features are mapped out onto the off-diagonal-block elements, and line shapes match excellently with the experimental data for transitions labeled by $\mathrm{LL}_{\mathrm{BLG}}$.

Figure 2 summarizes representative on-diagonal- and off-diagonal-block Mueller matrix difference spectra as a function of the magnetic field. The anisotropic resonance at 970 cm^{-1}, labeled with DTC, increases in amplitude with increasing magnetic field strength. The wave number, however, at which this resonance occurs does not vary with the external magnetic field strength. The physical origin of this resonance is the coupled motion of bound charge displacement near the longitudinal-optical phonon mode of the silicon carbide substrate with a free charge carrier plasma at the sample surface producing resonant magneto-optic birefringence [18,23,25]. Equations (1) and (2) can be used to render this phenomenon when $\hbar\omega_0$ is the (bound) phonon

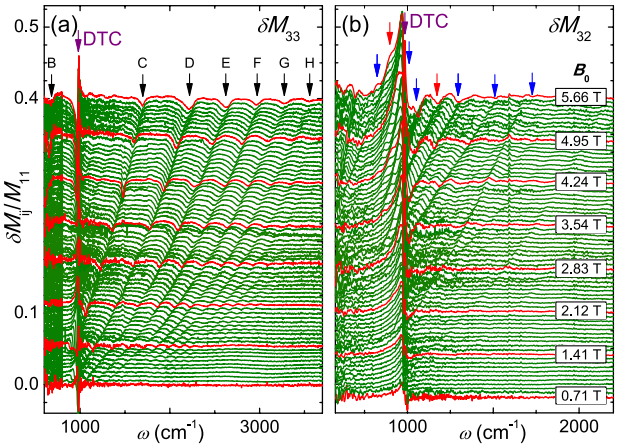

FIG. 2 (color online). Selected on- and off-diagonal-block optical Hall effect spectra ($T = 1.5$ K, $\Phi_a = 45°$) for $B_c = +(0.707 \pm 0.002)$ T to $B_c = +(5.66 \pm 0.02)$ T in 0.07 T increments. The graphs are stacked by 0.006. (a) δM_{33}: Isotropic inter-Landau-level transitions, indicated by letters according to Sadowski *et al.* [13]. (b) δM_{32}: Anisotropic inter-Landau-level transitions, indicated by blue and red arrows.

mode energy. The resulting polarization contribution is anisotropic and occurs in all Mueller matrix elements. We attribute this mode to highly doped graphene layers in the close vicinity of the interface between the substrate and the epitaxial graphene, originating from SiC charge transfer [26].

The magnetic field-dependent measurements reveal that energy spacings of transitions $\mathrm{LL}_{\mathrm{SLG}}$ scale with the square root of transition index n and magnetic field B, indicative for the Dirac-type band structure with Fermi level close to the charge neutrality point [13]. Data in Fig. 3(a) are

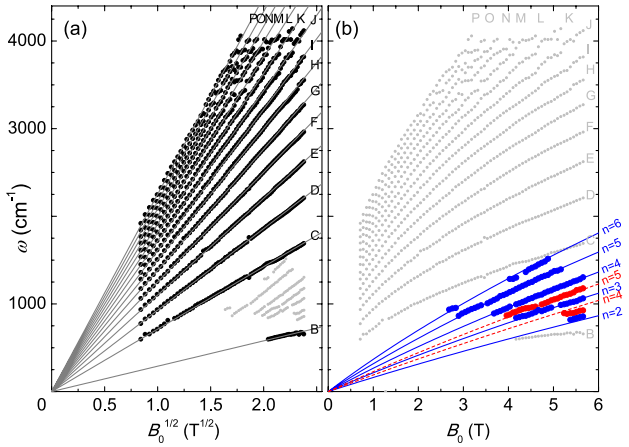

FIG. 3 (color online). Symmetric [(a) isotropic] and antisymmetric [(b) anisotropic] inter-Landau-level transition energies in epitaxial graphene determined from optical Hall effect measurements at 1.5 K. Solid lines denote single-layer graphene [(a) black solid lines and dots], bilayer graphene [(b) blue solid lines and dots], and trilayer graphene [(b) red dashed lines and dots] dependencies on the magnetic field.

parameters $\omega_{0,n}$ obtained from best-match model analysis of the optical Hall effect spectra as a function of B_c. We attribute these transitions to originate within regions of the epitaxial graphene that are composed of decoupled, quasi-neutral graphene sheets [14]. Energies in Fig. 3(a) follow $E_{\mathrm{SLG}}^{\mathrm{LL}}(n) = \mathrm{sgn}(n)E_0\sqrt{|n|}$ with $E_0 = \tilde{c}\sqrt{2\hbar e|B_c|}$ and average velocity of Dirac fermions $\tilde{c}$. The naming convention used to indicate transitions in Fig. 3(a) is adapted from Sadowski *et al.* [27]. Optical selection rules for transitions between levels n' and n require $|n'| = |n| \pm 1$. The best-match model velocity obtained from matching all data in Fig. 3(a) is $\tilde{c} = (1.01 \pm 0.01) \times 10^6$ m/s, in very good agreement with Refs. [4,13–15,28,29]. The corresponding best-match functions $E_{\mathrm{SLG}}^{\mathrm{LL}}$ versus B_c are plotted as solid lines in Fig. 3(a).

Transition energy parameters obtained from best-match model analysis of the off-diagonal-block optical Hall effect data are plotted in Fig. 3(b) and exhibit sublinear behavior. The magnetic field scaling of the energy spacings for the anisotropic transitions suggests bi- and trilayer graphene as their physical origin. The transition energies of N-layer graphene have been described as [15,30,31]

$$E_{N\text{-BLG}}^{\mathrm{LL}}(n,\mu) = \mathrm{sgn}(n)\frac{1}{\sqrt{2}}\left[(\lambda_N\gamma)^2 + (2|n|+1)E_0^2 + \mu\sqrt{(\lambda_N\gamma)^4 + 2(2|n|+1)E_0^2(\lambda_N\gamma)^2 + E_0^4}\right]^{1/2}, \quad (3)$$

with coupling constant γ, layer parameter λ_N [31], and where $\mu = -1, +1$ corresponds to the higher and lower subbands in the limit of zero magnetic field, respectively [31]. Optical selection rules are the same as for $E_{\mathrm{SLG}}^{\mathrm{LL}}(n)$. Using $\tilde{c} = (1.01 \pm 0.01) \times 10^6$ m/s, best-match model functions are plotted in Fig. 3(b) for $N = 2$ and $N = 3$ as blue (solid) and red (dashed) lines, respectively. No transition was observed that would correspond to $N > 3$. These transitions can be assigned to Bernal stacked bilayer graphene ($N = 2$) and trilayer graphene ($N = 3$). The best-match model parameters obtained here are $\gamma = (3120 \pm 175)\,\mathrm{cm}^{-1}$ for $N = 2$, corroborating the result obtained by Orlita *et al.* from Fourier-transform infrared transmission experiments [15]. For $N = 3$, we observe $\gamma = (3150 \pm 20)\ \mathrm{cm}^{-1}$, which renders the first experimental confirmation of the theoretical predictions by Koshino and Ando for trilayer graphene [31]. We note that these anisotropic inter-Landau-level transitions are only observed and resolved for $n = 2, \ldots, 6$ for bilayer graphene, and for $n = 4$ and $n = 5$ for trilayer graphene. At this point, we do not know why transitions with $n > 6$ for $N = 2$ and $n \neq 4$, $n \neq 5$ for $N = 3$ cannot be observed. However, the fact that these transitions appear with anisotropic optical Hall effect signatures suggests their coupling with free charge carriers within the sample. We propose that stacking order defects within the bilayer and trilayer graphene allows for coupling of Dirac particles within their Landau levels with the cyclotron resonance [9] of the free carrier plasma, resulting in anisotropic inter-Landau-level transition signatures.

The polarization selection rules are obtained here from polarization resolved measurements of the optical Hall effect instrument. The different polarization selection rules observed for the transitions labeled with SLG and BLG indicate that different physical processes contribute to their respective magneto-optic polarizability tensors. A possible mechanism using coupled or uncoupled bound or unbound electronic transitions was described above. According to this scenario, BLG transitions are affected by free charge carrier plasma oscillations whereas transitions SLG are not. The different coupling mechanisms for transitions in sets SLG and BLG can be concluded here from the knowledge of the polarization selection rules. We consider it worth noting that the polarization selection rules observed here for the different sets of inter-Landau-level transitions are invariant with respect to the magnetic field strength, over the range of magnetic fields observed here. This suggests that the mechanisms which lead to the different polarization selection rules, for example, the coupling of bound electronic transitions with magnetoplasma oscillations, are not affected by the magnetic field. This may change, however, at larger magnetic fields than those investigated here.

In conclusion, we find that inter-Landau-level transitions in epitaxial graphene grown on C-face SiC are governed by different polarization selection rules. The transitions belong to different sets, where each set possesses its own polarization selection rule. Hence, for a given magnetic field, the polarization behavior and selection rules can be used to differentiate the sets to which observed transitions belong. The polarization behavior can be obtained, for example, by reflection-type optical Hall effect measurements in the infrared spectral region. Specifically, for epitaxial graphene, two sets of transition series with polarization preserving as well as polarization mixing properties occur. We identify that the polarization preserving transitions originate from decoupled graphene monolayers, while the polarization mixing transitions originate from bilayer and trilayer graphene. This identification follows from observation of transitions belonging to equal polarization rules as a function of the magnetic field strengths. The polarization preserving and polarization mixing rules may find explanation by different coupling mechanisms of inter-Landau-level transitions with free charge carrier magneto-optic plasma oscillations.

The authors would like to acknowledge financial support from the Army Research Office (D. Woolard, Contract No. W911NF-09-C-0097), the National Science Foundation (Grants No. MRSEC DMR-0820521, No. MRI

DMR-0922937, No. EPS-1004094, and No. DMR-0907475), the University of Nebraska-Lincoln, the J. A. Woollam Foundation, the Office of Naval Research, the Swedish Research Council (VR) under Grant No. 2010-3848 and, the Swedish Governmental Agency for Innovation Systems (VINNOVA) under the VINNMER international qualification program, Grant No. 2011-03486.

*kuehne@huskers.unl.edu
http://ellipsometry.unl.edu

[1] C. Berger, Z. Song, T. Li, X. Li, A. Y. Ogbazghi, R. Feng, Z. Dai, A. N. Marchenkov, E. H. Conrad, P. N. First, and W. A. de Heer, J. Phys. Chem. B **108**, 19 912 (2004).
[2] C. Berger, Z. Song, X. Li, X. Wu, N. Brown, C. Naud, D. Mayou, T. Li, J. Hass, A. N. Marchenkov, *et al.*, Science **312**, 1191 (2006).
[3] C. Virojanadara, M. Syvaejarvi, R. Yakimova, L. I. Johansson, A. A. Zakharov, and T. Balasubramanian, Phys. Rev. B **78**, 245403 (2008).
[4] E. A. Henriksen, Z. Jiang, L.-C. Tung, M. E. Schwartz, M. Takita, Y.-J. Wang, P. Kim, and H. L. Stormer, Phys. Rev. Lett. **100**, 087403 (2008).
[5] A. Tzalenchuk, S. Lara-Avila, A. Kalaboukhov, S. Paolillo, M. Syväjärvi, R. Yakimova, O. Kazakova, T. J. B. M. Janssen, V. Fal'ko, and S. Kubatkin, Nat. Nanotechnol. **5**, 186 (2010).
[6] Y.-M. Lin, H.-Y. Chiu, K. A. Jenkins, D. B. Farmer, P. Avouris, and A. Valdes-Garcia, IEEE Electron Device Lett. **31**, 68 (2010).
[7] W. de Heer, C. Berger, M. Ruan, M. Sprinkle, X. Li, Y. Hu, B. Zhang, J. Hankinson, and E. Conrad, Proc. Natl. Acad. Sci. U.S.A. **108**, 16 900 (2011).
[8] Y. M. Lin, A. Valdes-Garcia, S. J. Han, D. B. Farmer, I. Meric, Y. N. Sun, Y. Q. Wu, C. Dimitrakopoulos, A. Grill, and P. A. K. A. Jenkins, Science **332**, 1294 (2011).
[9] I. Crassee, J. Levallois, A. L. Walter, M. Ostler, A. Bostwick, E. Rotenberg, T. Seyller, D. van der Marel, and A. B. Kuzmenko, Nat. Phys. **7**, 48 (2010).
[10] I. Crassee, J. Levallois, D. van der Marel, A. L. Walter, T. Seyller, and A. B. Kuzmenko, Phys. Rev. B **84**, 035103 (2011).
[11] Y. Q. Wu, K. A. Jenkins, A. Valdes-Garcia, D. B. Farmer, Y. Zhu, A. A. Bol, C. Dimitrakopoulos, W. J. Zhu, F. M. Xia, P. Avouris, and Y. M. Lin, Nano Lett. **12**, 3062 (2012).
[12] T. Morimoto, M. Koshino, and H. Aoki, Phys. Rev. B **86**, 155426 (2012).
[13] M. L. Sadowski, G. Martinez, M. Potemski, C. Berger, and W. A. de Heer, Phys. Rev. Lett. **97**, 266405 (2006).
[14] M. Orlita, C. Faugeras, P. Plochocka, P. Neugebauer, G. Martinez, D. K. Maude, A.-L. Barra, M. Sprinkle, C. Berger, W. A. de Heer, and M. Potemski, Phys. Rev. Lett. **101**, 267601 (2008).
[15] M. Orlita, C. Faugeras, R. Grill, A. Wysmolek, W. Strupinski, C. Berger, W. A. de Heer, G. Martinez, and M. Potemski, Phys. Rev. Lett. **107**, 216603 (2011).
[16] T. Hofmann, U. Schade, C. M. Herzinger, P. Esquinazi, and M. Schubert, Rev. Sci. Instrum. **77**, 063902 (2006).
[17] T. Hofmann, C. M. Herzinger, J. L. Tedesco, D. K. Gaskill, J. A. Woollam, and M. Schubert, Thin Solid Films **519**, 2593 (2011).
[18] M. Schubert, T. Hofmann, and C. M. Herzinger, J. Opt. Soc. Am. A **20**, 347 (2003).
[19] T. Hofmann, C. Herzinger, C. Krahmer, K. Streubel, and M. Schubert,, Phys. Status Solidi (a) **205**, 779 (2008).
[20] H. Fujiwara, *Spectroscopic Ellipsometry* (Wiley, New York, 2007).
[21] J. L. Tedesco, G. G. Jernigan, J. C. Culbertson, J. K. Hite, Y. Yang, K. M. Daniels, R. L. Myers-Ward, C. R. Eddy, J. A. Robinson, K. A. Trumbull, *et al.*, Appl. Phys. Lett. **96**, 222103 (2010).
[22] A. Boosalis, T. Hofmann, V. Darakchieva, R. Yakimova, and M. Schubert, Appl. Phys. Lett. **101**, 011912 (2012).
[23] M. Schubert, *Infrared Ellipsometry on Semiconductor Layer Structures: Phonons, Plasmons and Polaritons*, Springer Tracts in Modern Physics Vol. 209 (Springer, Berlin, 2004).
[24] T. E. Tiwald, J. A. Woollam, S. Zollner, J. Christiansen, R. B. Gregory, T. Wetteroth, S. R. Wilson, and A. R. Powell, Phys. Rev. B **60**, 11 464 (1999).
[25] M. Schubert, T. Hofmann, and J. Šik, Phys. Rev. B **71**, 035324 (2005).
[26] Y.-M. Lin, C. Dimitrakopoulos, D. B. Farmer, S.-J. Han, Y. Wu, W. Zhu, D. K. Gaskill, J. L. Tedesco, R. L. Myers-Ward, J. Charles, R. Eddy, A. Grill, and P. Avouris, Appl. Phys. Lett. **97**, 112107 (2010).
[27] M. Sadowski, G. Martinez, M. Potemski, C. Berger, and W. de Heer, Solid State Commun. **143**, 123 (2007).
[28] M. Orlita, C. Faugeras, J. Borysiuk, J. M. Baranowski, W. Strupiński, M. Sprinkle, C. Berger, W. A. de Heer, D. M. Basko, G. Martinez, and M. Potemski, Phys. Rev. B **83**, 125302 (2011).
[29] M. Orlita, C. Faugeras, J. M. Schneider, G. Martinez, D. K. Maude, and M. Potemski, Phys. Rev. Lett. **102**, 166401 (2009).
[30] D. S. L. Abergel and V. I. Fal'ko, Phys. Rev. B **75**, 155430 (2007).
[31] M. Koshino and T. Ando, Phys. Rev. B **77**, 115313 (2008).